

RSC Advances



This is an *Accepted Manuscript*, which has been through the Royal Society of Chemistry peer review process and has been accepted for publication.

Accepted Manuscripts are published online shortly after acceptance, before technical editing, formatting and proof reading. Using this free service, authors can make their results available to the community, in citable form, before we publish the edited article. This *Accepted Manuscript* will be replaced by the edited, formatted and paginated article as soon as this is available.

You can find more information about *Accepted Manuscripts* in the [Information for Authors](#).

Please note that technical editing may introduce minor changes to the text and/or graphics, which may alter content. The journal's standard [Terms & Conditions](#) and the [Ethical guidelines](#) still apply. In no event shall the Royal Society of Chemistry be held responsible for any errors or omissions in this *Accepted Manuscript* or any consequences arising from the use of any information it contains.

Structural, optical and electrical characterizations of gadolinium and indium doped cadmium oxide/*p*-silicon heterojunction for solar cell applications

L. L. Pan, K. K. Meng, G. Y. Li, H. M. Sun, J. S. Lian*

Key Laboratory of Automobile Materials, College of Materials Science and Engineering, Jilin University, Nanling Campus, Changchun 130025, China

Abstract

The gadolinium and indium co-doped CdO thin films were prepared by pulsed laser deposition method. The XRD and XPS results indicated that Gd^{3+} and In^{3+} ions occupied the locations in interstitial positions and/or Cd^{2+} -ion vacancies in CdO lattice. The FESEM images showed that the films were homogeneous and consisted of nanograins with a size range of 23~40 nm. The optical band gap of CdO thin films can be engineered over a wide range of 2.72~3.56 eV by introducing Gd and In dopant. Such transparent semiconducting Gd and In co-doped CdO films were then grown on *p*-type Si substrates to fabricate the *n*-CdO/*p*-Si heterojunction devices. The important junction parameters such as the series resistance (R_s), ideality factor (n) and Schottky barrier height (Φ_b) were determined by performing different plots from the current density-voltage (J - V) characteristics. The obtained results indicated that the electrical properties of the heterojunction diodes were controlled by the dopant concentration. The *p*-Si/*n*- $\text{Cd}_{1-x-y}\text{Gd}_x\text{In}_y\text{O}$ heterojunction diode showed the best values of open circuit voltage, $V_{oc} = 1.04$ V and short circuit current density, $J_{sc} = 11.4$ mA/cm² under an illumination intensity of 100 mWcm⁻², which was suitable for solar cell applications.

Keywords: CdO thin film; Gadolinium; Indium; Heterojunction; Electrical properties; PLD method.

* Corresponding author at: The Key Lab of Automobile Materials, Ministry of Education, College of Materials Science and Engineering, 5988 Renmin Street, Jilin University, Nanling Campus, Changchun 130025, Jilin, P.R. China.

Tel.: +86 431 85095875; fax: +86 431 85095876.

E-mail address: lianjs@jlu.edu.cn (J.S. Lian).

1. Introduction

Metal-oxide semiconductors such as ZnO^[1], CdO^[2], SnO₂^[3] and TiO₂^[4] etc. have been used extensively for optoelectronic applications such as solar cells, energy-efficient windows, flat panel displays (FPDs), light emitting diodes and other optoelectronic devices^[5-7]. Among these semiconductors, CdO is an n-type semiconductor with a direct band gap of 2.2 eV, and is the suitable material for band gap engineering and as well as for p-n junction applications. CdO has received a considerable attention for photovoltaic applications on account of its relatively low electrical resistivity ($10^{-2}\sim 10^{-4}$ Ω cm) and high optical transparency in the visible range of solar spectrum wavelength range^[8]. Different physical and chemical deposition techniques such as spray pyrolysis^[9], sol-gel^[10], magnetron sputtering^[11], chemical bath deposition (CBD)^[12], pulsed laser deposition (PLD)^[13], metal-organic chemical vapor deposition (MOCVD)^[14] etc. have been employed to prepare undoped and doped CdO thin films. There are several reports on improving the optical band gap and electrical conductivity of CdO by doping the metallic elements. Zheng et al.^[15] have showed an increase in optical band gap up to 2.93 eV for Sn-doped CdO thin films using PLD method. Yang et al.^[16] have prepared CdIn₂O₄ thin films

using DC magnetron sputtering, and the lowest resistivity of $2 \times 10^{-4} \Omega \text{ cm}$ was obtained for the films annealed in nitrogen. The rare earth oxides are potential doping candidate to improve the optical transparency and band gap of conducting metal oxides because of their wide optical band gap^[17]. Gupta et al.^[18] have observed that an increase in optical band gap up to 3.4 eV by doping 2 at. % Gd in CdO film grown at low temperature (373 K) and oxygen pressure of 1×10^{-5} mbar using PLD method, and the lowest electrical resistivity of $2.71 \times 10^{-5} \Omega \text{ cm}$ and the highest mobility of $258 \text{ cm}^2/\text{Vs}$ was achieved. Moreover, the electrical characterizations of CdO Schottky devices or heterojunction diodes fabricated by different methods have been investigated. Since the use of heterostructure can provide an advantage in the control of the electronic and optoelectronic properties of semiconductor devices, some reproducible and stable CdO-based p-n heterojunctions with sufficiently high power conversion efficiency have been fabricated and their photodiode properties have been studied. Especially, the heterojunction diodes made from CdO thin layers on crystalline silicon are particularly interesting due to their more cost effectiveness and flexibility for optoelectronic device fabrications. The n-CdO/p-Si heterojunction diodes show very good spectral response at both the infrared and blue regions of the visible wavelength. These diodes require a low reverse voltage in order to achieve a high illumination response.

In this work, nanostructured Gd and In co-doped CdO thin films were prepared by pulsed laser deposition (PLD) method and their microstructures and optical properties were analyzed. Then, the Gd and In co-doped CdO thin layer was deposited on *p*-Si substrate to construct a *n*-CdO:Gd:In/*p*-Si heterojunction device for solar cell application. The electrical properties of the heterojunction devices with different Gd and In doping concentrations have been

investigated by means of current density-voltage (J - V) measurements. The heterojunction diodes showed good rectification behavior, and the ideality factor and barrier height values were found to be low. A dominant open circuit voltage and short circuit current density were obtained in the n -Cd_{0.81}Gd_{0.03}In_{0.06}O/ p -Si heterojunction diode with good power conversion efficiency under a simulated solar light exposure.

2. Experimental

The targets for PLD were prepared by a standard solid-state reaction using high purity (99.99 %) of CdO, Gd₂O₃ and In₂O₃ powders. The doping ratio of Gd: In was selected to be 1:2. So, the powders were prepared with Gd atomic concentration (x) of 1 %, 2 % and 3 %, and the corresponding In atomic concentration (y) of 2 %, 4 % and 6 %, respectively. The required amounts of CdO, Gd₂O₃ and In₂O₃ were weighed accurately and mixed thoroughly. The powder mixture was cold pressed to make disks under a hydraulic pressure of 6 MPa and then sintered at 1173 K in air for 12 h to make targets. The undoped CdO and CdO doped with Gd & In (CGIO) thin films were prepared at 473 K for 10 min. Pulsed Nd: YAG laser with a wavelength of 1064 nm is used. The repetition rate is 10 Hz and the fluency on target is set at 16 J/cm² for all samples. The distance between the target and the substrate is kept at 3.0 cm. The chamber was evacuated first to a base pressure below 5×10^{-4} Pa using a turbo molecular pump and then filled with oxygen to a pressure of 10 Pa. The quartz glass substrates were cleaned successively by ethanol, acetone and deionized water, respectively. The p -type silicon wafer is single crystal (100) silicon with a thickness of 500~550 μ m and a resistance of 5~8 Ω . The native oxide on the polish surface of the silicon wafer was removed in HF: H₂O (1:10) solution.

The crystal structure of the sample films was analyzed by X-Ray Diffraction (XRD)

(Rigaku Dymax) with a Cu target and a mono-chromometer at 40 kV and 250 mA. The chemical composition of the samples was analyzed by X-ray photoelectron spectroscopy (XPS) with an ESCALAB Mk II (Vacuum Generators) spectrometer using non-monochromatic Al K α radiation (240 W). The surface morphology of the samples was characterized using Cold field emission scanning electron microscope (FESEM, JSM-6700F), and the thickness of the samples was determined to be about 170 nm. The optical properties of the films were characterized by a UV-visible spectrophotometer (UV-6100PC). The electrical conductivity of the CdO films was carried out with a standard Van-der-Pauw method using an Accent HL5500 Hall System. The electrical measurements of *n*-CdO/*p*-Si heterojunction diodes were carried out by a Keithley 2400 source meter under simulated AM1.5 G illumination (100 mWcm⁻²) provided by a solar light simulator (Oriel, Model: 91192). The ohmic contacts were formed by sputtering Ag metal on the back of Si wafer and Al metal on the top of the *n*-type CdO films. A shadow mask was used during sputtering to define the active area of 3.14 mm². The schematic diagram of an Al/*n*-CdO/*p*-Si/Ag heterojunction diode was shown in Figure 1.

3. Results and discussion

3.1 Structural characterization

Figure 2 shows the XRD patterns of undoped CdO and CGIO films. The observed diffraction patterns show the polycrystalline nature of CdO with cubic (Fm3m) structure^[19], with the preferred orientation growth on (200) plane. None of Gd₂O₃ and In₂O₃ diffraction peaks from CGIO films are detected, indicating that Gd and In atoms have been doped into CdO lattice. The weakening of other diffraction peaks than (200) plane for the CGIO films indicates the further enhancement of the preferred orientation growth on (200) plane, which would be in

favor of the improvement of crystallinity of the CGIO thin films, as shown by the intensity increase of their (200) diffraction peaks. Some structural parameters, such as dislocation density (δ), microstrain (ε), stress (σ) and stacking fault (SF) are calculated from the XRD spectra^[20]. The results show that the values of ε increase from 1×10^{-3} to 1.64×10^{-3} , they are very small in the order of 10^{-3} . And the values of δ , σ and SF increase from 8.26×10^{14} line m^{-2} , 84.5 MPa and 0.428 to 2.12×10^{15} line m^{-2} , 138.6 MPa and 0.43, respectively. The increase in lattice parameters suggests that the introduction of Gd^{3+} and In^{3+} can promote the dislocations concentrate on the grain boundaries, and then lead to the relaxation of grain boundary.

The representative XPS spectra are shown in Figure 3a. All of the peaks are calibrated by using C 1s (284.6 eV) as the reference. The narrow scan spectra of Cd 3d are shown in Figure 3b, where the Cd 3d features of CdO film consist of the main $3d_{5/2}$ and $3d_{3/2}$ spin-orbit components at 405.1 eV and 411.8 eV, respectively, while the peaks of Cd $3d_{5/2}$ and Cd $3d_{3/2}$ of the CGIO films shift slightly to lower energies of 404.8 eV and 411.5 eV, respectively, indicating the substitutions of Cd atoms by Gd and In atoms in the CdO lattices. The characteristic peak of Gd $4d_{5/2}$ at 141.8 eV is observed for CGIO films shown in Figure 3c, which indicates that Gd^{3+} ions exist in the positions of Cd^{2+} ions and the peak intensity increases with increasing Gd concentration. The characteristic peaks of In $3d_{5/2}$ and In $3d_{3/2}$ at 444.2 eV and 452.4 eV, respectively, are also observed (Figure 3d), confirming also that In^{3+} ions exist in these CGIO films. The O 1s peak with peak deconvolution after background removal by the Shirley method is shown in Figure 4. All CdO and CGIO films have three components of oxygen with different binding energies: O (II): 530.75 ± 0.15 eV, O (III): 531.54 ± 0.20 eV, and O (IV): 532.17 ± 0.15 eV, which correspond to the O-Cd bonds, the O^{2-} ions

in the oxygen deficient regions within the matrix of CdO and surface absorbed oxygen (incorporation of $(O_2)^{2-}$ peroxy species^[21], respectively. There is also an O (I) component unique to the CGIO films (Figure 4b~d), which is the O 1s spectrum coming from In_2O_3 ^[22] and the peak is more clear in the spectra of CGIO films with 3 % Gd and 6 % In.

The concentrations of gadolinium and indium can be measured from the XPS results. The measured concentrations in the films and the nominal concentrations in the target of gadolinium and indium are shown in Table 1, both are comparable although the measured concentrations are little lower than the nominal concentrations in the targets. The ratios of [O]/ [Cd] for these films are also calculated from the XPS results and shown in Table 1. All the ratios are smaller than unity, which confirms the oxygen deficiency in the films. The induced oxygen vacancies serve as shallow donors and are responsible for the n-type conductivity of the films. In addition, with an increase in Gd and In concentrations, the values show an increased trend which implies the decreased deficiency of oxygen in the films, it is due to the substitutions of Cd^{2+} by either In^{3+} or Gd^{3+} ions in the CdO lattice.

The microstructure of semiconductor films has an important effect on the electrical performance for the heterojunction diodes. Typical FESEM images of the CdO and CGIO thin films are displayed in Figure 5a~d. As shown, all the films are composed of nanograins. The undoped CdO film (Figure 5a) exhibits a dense morphology with randomized small particles with an average grain size of 40 nm. With the introduction of Gd and In, the films (Figure 5b~d) become more smooth, continuous, homogeneous and compact, and the average grain size decreases gradually to 37, 26 and 23 nm, respectively, with increasing Gd and In concentrations. The obvious decrease in the grain size may be attributed to the existence of internal strain and

lattice distortion or defects induced by the dopant. As the atom size of Gd (2.54 Å) or In (2.00 Å) is larger than that of Cd (1.71 Å), the doping of Gd and In will induce lattice distortion, and the dopant atoms prefer to dwell in/near grain boundary regions in order to reduce lattice distortion. So, more Gd and In atoms locating in/near grain boundaries would prevent grain growth. Therefore, an obvious decrease in grain size is observed for the Gd and In doped CdO films.

3.2 Optical and electrical characterization

The optical transparency and band gap of a semiconductor film are very important parameters for their optoelectronic and photovoltaic applications. The optical transmission spectra of CdO and CGIO films are shown in Figure 6. The optical transmission of the film increases from 83 % to 92 % in visible spectral region as Gd and In doping level increases. With an increase in Gd and In concentrations, a blue shift in the absorption edge of the film is noteworthy as it leads to an increase in the width of transmission window. The direct optical band gap (E_g) is obtained by a careful analysis of absorption coefficients^[23], and it can be determined by extrapolating the linear regions of the plots to zero absorption (see the insert in Figure 6). It is seen that the doping of Gd and In induces an evident increase of band gap (E_g), for example, from 2.72 eV for undoped CdO film to 3.56 eV for the CGIO film with 2 % Gd and 4 % In. In general, the conduction characteristics of CdO film are dominated primarily by the electrons generated from oxygen vacancies and Cd interstitial atoms. Compared with the undoped CdO film, doped Gd³⁺ and In³⁺ ions on substitution sites of Cd²⁺ ions or in interstitial sites of the CdO lattice will provide more electrons and holes and hence increase the carrier concentration, which would widen the band gap according to the Burstein-Moss (B-M) effect^[24-25]. However, with the content of Gd and In increasing to 3 % and 6 %, respectively, the

band gap decreases inversely to 3.26 eV. This sudden shrinkage in heavy donor doping may be attributed to the comprehensive effect of the band gap renormalization, the formation of impurity phase, and localization effect of transition metal. Firstly, the band gap renormalization can be caused by the electron-dopant interactions and electron-electron Coulomb and exchange interactions within the conduction band. Similar shrinkage of band gap is also observed with other trivalent dopants (Y, Sm, Dy, Sc and Al). Moreover, the 4*f*-electrons of the impurity dopant ions can add a new parameter (like 4*f*-5*d* transition) to the energy band spectrum of CdO. Thus, due to the doping of Gd³⁺ and In³⁺, the band tailing or impurity band becomes broader and reaches finally and merges the bottom of the conduction band causing the sudden decrease in the band gap. Secondly, according with the XPS analysis, oversaturated indium atoms are precipitated at grain boundary to form impurity phase of In₂O₃, which act as defect levels to appear between the valence and conduction band of CdO and caused finally the optical band gap decreasing. Thirdly, as the substitute of Cd²⁺ ions, the 5*d*-electrons of In³⁺ ions can engender a spin exchange interaction with the electrons of the semiconductor band edge and then the optical band gap begin to red shift. Due to these reasons, a decrease in band gap is observed for over doping of Gd and In. Despite all of these, the band gap values of all the CGIO films are optimum match for the solar spectrum.

From Table 2, it is observed that the doping of Gd and In can cause a marked reduction in the resistivity. With an increase in Gd and In concentrations, the resistivity of the films decreases from $2.48 \times 10^{-3} \Omega\text{cm}$ to $7.6 \times 10^{-5} \Omega\text{cm}$. The decrease in resistivity can be also associated with the increase in carrier concentration from $1.08 \times 10^{20} \text{cm}^{-3}$ to $1.47 \times 10^{21} \text{cm}^{-3}$ and the mobility from $77.5 \text{cm}^2/\text{Vs}$ to $115.9 \text{cm}^2/\text{Vs}$. The enhanced conductivity plays a very

important role in the successful fabrication of the Schottky diodes. The low resistivity of the CdO films will lead to a wide depletion width at the junction between the CGIO layer and Al electrode, which can restrain the tunneling current through the barrier and obtain a good rectifying effect.

3.3 Current-voltage characteristics of the Al/n-CdO/p-Si/Ag heterojunction diode

The current density-voltage (J - V) characteristics of the CdO/p-Si and CGIO/p-Si heterojunction diodes under dark condition are shown in Figure 7. All the curves are asymmetrical and non-linear. These diodes exhibit good rectification behavior. The rectification ratio (RR) is calculated as the ratio of forward current density (J_F) to the reverse current density (J_R) at a certain applied voltage (V), i.e., $RR = (J_F/J_R)_v$. The plots of RR versus V for the diodes are shown in the inset of Figure 7. The RR values are found to be dependent on the dopant concentrations and the applied bias. The grain boundary scattering-limited mobility plays an important role in the decreased in RR values, this poor transport properties could not provide effectively a direct electrical pathway for the electrons. It can also be seen that the currents increase linearly at lower applied voltages (0.1~0.4 V), it suggests an ohmic conduction. With the increase of applied voltage (0.4~2.0 V), the forward currents follow approximately an exponential trend. Typical logarithmic plots of the J - V characteristics at relatively high forward voltage regions are shown in Figure 8. As shown, the current density can be expressed by a power-law, i.e., $J \propto V^m$. The curve (Figure 8 inset) shows that the m values calculated from the slopes in Figure 8 decrease from 2.23 to 1.97. The obtained results ($m \approx 2$) suggest a space current limited current (SCLC) conduction mechanism corresponding to the case where no traps are present or all traps are filled, and in SCLC region, the current increases

quadratically with the bias voltage. The experimental values of Schottky barrier height (Φ_b) and ideality factor (n) are determined from the current axis intercept and the slope of the linear region of the forward bias semi-log J - V curve, respectively^[26]. The calculated values are presented in Table 3. It shows that with the increase in Gd and In doping concentrations, the n values decrease from 2.27 to 1.69, while the Φ_b values increase from 0.55 to 0.61 eV. The obtained n values confirm the presence of a combination of recombination and diffusion currents in these diodes, and the decrease in ideality factor may be attributed to the improved interface state of $\text{Cd}_{1-x}\text{Gd}_x\text{In}_y\text{O}/p$ -Si diodes. It is consistent with the XPS analysis (Table 3 and Figure 4), and it shows that there are fewer oxygen-related defect centers in the CGIO films. This improvement can greatly reduce the defect-assisted tunneling probability. The increase in values of the Φ_b is mainly due to fewer low Schottky barrier height regions with Gaussian distribution existing at the interface, and more electrons have sufficient energy to overcome the Φ_b when dopant concentrations increase. Moreover, the deviations in the ideality factor may be due to the spatially inhomogeneous barrier height and the potential fluctuations at the interface that consist of the low and high barrier heights^[27-28], i.e. the current through the diode will flow preferentially through the lower barriers in the potential distribution. So, the interface states play an important role on determination of Schottky barrier height and other electronic parameters and these can affect diode performance, stability and reliability. The largest value of Φ_b (0.61 eV) in present work is found to be smaller than 0.87 eV reported by Siad et al.^[28] and Sağlam et al.^[29] for the Al/ p -Si Schottky barrier diodes. The case may be ascribed to CdO or CGIO films modifying the effective barrier height by influencing space charge region of the Si substrate. On the other hand, for this metal oxide semiconductor/ p -Si heterostructure diodes,

the results obtained by Farag. et al.^[30] are slightly inferior to ours. He has shown that the values of n and Φ_b were 2.1 and 0.68 eV for 2 at. % Zn doped CdO/ p -Si diodes, respectively.

The series resistance (R_s) and shunt resistance (R_{sh}) are determined from the plot of junction resistance (R_j), against voltage (V), where $R_j = \partial V/\partial J$, as shown in Figure 7. The obtained data are presented in Table 3. It clearly shows that with the increase in the dopant concentrations, the R_s value increases from 161.2 to 689.3 $\Omega\cdot\text{cm}^2$, which may be attributed to the increase in the number of free charge carriers, by either bond breaking or de-trapping mechanism^[31], and the R_s really plays an important current-limiting role for this heterostructure. The R_{sh} reflects the existence of defects that provide forward leakage path to minority charge carriers and grain boundaries are the source of the defects in case of polycrystalline materials. So, the FESEM image in Figure 5d shows the increase of defects due to Gd and In doping, it can explain the reason why the R_{sh} value increases from 6.2×10^3 to 2.2×10^4 $\Omega\text{ cm}^2$.

3.4 Photovoltaic properties of Al/ p -Si/ n -CdO/Ag heterojunction diode

The current density-voltage characteristics of the heterojunction diodes under an illumination intensity of $100\text{ mW}\cdot\text{cm}^{-2}$ are showed in Figure 9. It can be seen that the current under illumination is higher than the dark current by about one or two order of magnitude. It is mainly due to the generated electron-hole pairs, i.e. neutral excitons, and these charges contribute to the photocurrent as a result of the light absorption. The light illumination does not change significantly the forward current of the diodes, whereas the current in the reverse direction is increased by illumination. It indicates that the rectification effect is weakened and the diodes exhibit more ideal behavior under illumination. With an increase in the doping concentrations, the number of photo-generated carrier charges is increased at the interface, the

$\text{Cd}_{1-x-y}\text{Gd}_x\text{In}_y\text{O}$ layer absorbs the photons (Figure 10) and the photo-generated carriers are sufficiently energetic to cross the barrier height, and this leads to high jump probability of charge carriers between CdO or CGIO film and Si layer. Moreover, the $\text{Cd}_{1-x-y}\text{Gd}_x\text{In}_y\text{O}$ film has better transparency for the visible light and allows more light transmit into the Si layer. Thus, the diodes become more sensitive to light, that is, the addition of Gd and In gives a rise of the photocurrent. The R_s and R_{sh} in the photovoltaic diode are mainly influenced by the movement of photocurrent. They are calculated from Figure 9 and also compiled in Table 3. As shown, the values of R_s and R_{sh} decrease significantly by one to three orders of magnitude than those obtained in dark. With the increase in doping levels, the R_s value decreases from 34.5 to 11.8 $\Omega \text{ cm}^2$, and the R_{sh} value also decreases from 483.9 to 46.2 $\Omega \text{ cm}^2$. For the best diode performance, the highest R_{sh} value and the lowest R_s value are desired. So, though the R_{sh} values of our diodes are still higher than those of the R_s values, but the low R_{sh} values can cause power losses in diodes by providing an alternate current path for the photo-generated current. The filling factor (FF) and conversion efficiency (η) can be calculated by the solar cell parameters^[32]. These parameter, such as open circuit voltage (V_{oc}), short-circuit current density (J_{sc}), current density (J_m) and potential maximum power point (V_m) can be observed directly in the inset of Figure 9. And the calculated results can also be seen in Table 3. The results indicate that the heterojunction solar cells have good photovoltaic abilities. The V_{oc} for the undoped CdO is found to be close to that of conventional Si solar cells. With the increase in dopant concentrations, the V_{oc} value increase from 0.49 to 1.04 V and the J_{sc} value increase consistently from 0.8 to 11.4 mA/cm^2 . The highest value of V_{oc} for the studied diodes is higher than those of previous reported heterojunction solar cells^[33-36]. The detailed comparison is

presented in Table 4. The remarkable improvement in J_{sc} in our case may be strongly related to the enhancement of the diffusion (built-in) potential (Φ_{bi}). The Schottky barrier height (Φ_b) and the diffusion potential (Φ_{bi}) can be consistently explained by the following equation: $\Phi_b = E_c - E_f + \Phi_{bi}$, we tentatively assume that the potential difference of the Fermi level (E_f) and the top of the conduction band in the Si layer are constant, so Φ_{bi} is increased with the increase in Φ_b . Due to the enhancement of Φ_{bi} , more photo-generated electron-hole pairs diffused at the interface of $Cd_{1-x}Gd_xIn_yO/p$ -Si are dissociated rapidly. Thus, more separated electrons (or holes) are transported towards the cathode (or anode) and then the larger J_{sc} can be collected. Moreover, the lattice mismatch and different thermal expansion coefficient between $Cd_{1-x}Gd_xIn_yO$ film and Si layer can induce the interface defects generation. However, it can be seen from the XRD and XPS analysis that the preferential orientation of (200) plane increases constantly and the oxygen vacancies decrease continually with the increase in doping levels. The comprehensive effect of these factors will cause a decrease in the interface defects and the charge recombination centers in space charge region, and then lead to the recombination current decreases gradually. Thus, the successful suppression of charge recombination is favorable for J_{sc} increasing. Similarly, the modified interface state correlates with the continuing increased V_{oc} , because V_{oc} is affected significantly by the trapping sites and charge recombination centers existing at the interface and grain boundary of the CGIO film. As these defects decrease continuously, the kinetic balance between electron photogeneration and loss achieves gradually optimal effect. That is, the higher crystallinity property and carrier density for the CGIO film, the faster photo-generated electrons transport to the anode contact. Thus, the shortened electron pathway and prolonged electron lifetime can reduce the charge recombination loss, and then

increase greatly V_{oc} for the photodiodes. In addition, the reduction of R_s in the diodes can further ensure a higher V_{oc} due to the decrease of the potential drop at the interface of active layer and cathode. Along with the enhancement of V_{oc} and J_{sc} , the FF value increases from 51 % to 63 %, for laboratory cells, the FF value is expected to be over 70 % and the decrease in modules is indicative of higher series resistance. In general, a recombination current during the photovoltaic operation might suppress the power conversion efficiency. In our research, the power conversion efficiency (η) increases from 0.6 % to 7.5 %, it suggests that the interface states are improved and/or the interfacial oxide layer is decreased, consequently, electron transport would become faster and thus boost the charge transfer efficiency. The comparison in Table 4 shows that although the power conversion efficiency has been improved greatly by doping of Gd and In, our value is not the highest. The lattice mismatch between CdO (CGIO) film and Si layer may also decrease the power conversion efficiency.

To compare the relative photoconductivity sensitivity of the device to the illumination, the current sensitivity or optical response $S = [I_{Ill} - I_{Dark}] / [P_{In}]$ (mA/W) is used, where I_{Ill} and I_{Dark} are the currents measured at 2 V forward voltages under illumination and in dark, respectively. The results can also be seen in Table 3. The S value increases from 45.6 mA/W to 1708 mA/W with the increase in Gd and In doping levels, it means that dopants make an important contribution to the electrical and optical properties of the n -CdO/ p -Si diodes. So, our study may open the possibilities of systematic research and further development in the Al/ p -Si/ n -CdO/Ag photovoltaic device.

3.5 The band structure of the heterojunction diode

The band structure of n -CdO/ p -Si heterojunction diode can be constructed using Anderson model^[37]. In the construction of the band structure, the effect of interfacial state and variance of the Fermi energy are neglected. Figure 11 shows the constructed band structure of the n -CdO (CGIO)/ p -Si heterojunction diode under forward bias. In this diagram, the values of band gap of E_g (CdO/CGIO) = 2.82~3.56 eV and E_g (Si) = 1.12 eV, the electron affinity for CdO, χ (CdO) = 4.51 eV and the electron affinity for Si, χ (Si) = 4.05 eV are used. As shown, the conduction-band offset is $\Delta E_c = \chi$ (CdO) - χ (Si) = 0.46 eV, and the valance-band offset is $\Delta E_v = E_g$ (CdO/CGIO) - E_g (Si) + $\Delta E_c = 2.16$ ~ 2.9 eV. ΔE_v has a higher value than the ΔE_c . This means that, the energetic barrier for electrons is much lower than that for holes; therefore, the injection of electrons from n -CdO (CGIO) to p -Si is greater than the holes injection from p -Si to n -CdO (CGIO). Under forward bias, electrons can be more easily injected into the p -Si side because of the smaller potential barrier. Therefore, the forward current increases rapidly under a higher voltage bias. Moreover, the injection of electrons into p -Si widens the depletion layer on n -CdO and retards holes injection, leading to early current saturation.

4. Conclusions

Highly transparent and conductive Gd and In doped films were deposited on the quartz glass substrates at 473K by the pulsed laser deposition method, and the as-deposited CGIO films and p -Si wafer were used as n -type and p -type semiconductors to fabricate the Al/ n -Cd_{1-x-y}Gd_xIn_yO/ p -Si/Ag heterojunction diode. Several conclusions can be derived.

1. The XRD and XPS results indicated that Gd³⁺ and In³⁺ ions occupied locations in interstitial positions and/or Cd²⁺ ion vacancies. All the thin films were homogeneous and the size of nanograins decreased from 40 nm to 23 nm with the introduce of Gd and In.

2. The optical band gap of CdO thin film increased firstly from 2.72 to 3.56 eV and then decreased to 3.26 eV by introducing Gd and In dopant. The band gap widening of CGIO thin films can be well explained by the combination of band gap renormalization and Burstein-Moss effect. The high optical transparency (~85 %) and widened band gap can render the nanostructured CGIO thin film a promising candidate for optoelectronic applications.
3. The electrical properties of the Al/n-Cd_{1-x-y}Gd_xIn_yO/p-Si/Ag heterojunction diodes have been investigated by current density-voltage (*J-V*) characteristics. The dark *J-V* characteristics of the diodes showed a rectification behavior. At lower voltages, the dark forward *J-V* characteristics can be explained on the basis of thermionic conduction mechanism, while at higher forward voltages, the dark current was space charge limited conduction (SCLC) dominated by a single trap level with exponential traps. The reverse bias current density was interpreted in terms of the Schottky mechanism. With the increase in doping levels, the ideality factor (*n*) of diodes decreased gradually from 2.27 to 1.69, and exhibited more ideal behavior.
4. Under illumination with intensity of 100 mW·cm⁻², the Al/3 % Gd and 6 % In doped CdO/p-Si/Ag heterojunction diode showed the best values of open circuit voltage, $V_{oc} = 1.04$ V and the short circuit current density, $J_{sc} = 11.4$ mA/cm². Along with the enhancement of J_{sc} and V_{oc} , the filling factor (*FF*), power conversion efficiency (*η*) and current sensitivity (*S*) of diodes also increased with increasing doping concentrations. This may endue Al/CGIO/p-Si/Ag heterojunction diode the possibility of further development in photovoltaic device or solar cell application.

Acknowledgments

This work was supported by the Foundation of National Key Basic Research and Development Program (No. 2010CB631001), the National Nature Science Foundation (Grant No. 31070841) and the Program for Changjiang Scholars and Innovative Research Team in University.

References

- [1] S.J. Clark, J. Robertson, S. Lany, A. Zunger, *Phys. Rev. B.*, 2010, 81, 115311.
- [2] I. Akyuz, S. Kose, E. Ketenci, V. Bilgin, F. Atay, *J. Alloys Compd.*, 2011, 509, 1947.
- [3] A.K. Singh, A. Janotti, M. Scheffler, C.G. Van de Walle, *Phys. Rev. Lett.* 2008, 101, 055502.
- [4] X. Chen, S.S. Mao, *Chem. Rev.*, 2007, 107, 2891.
- [5] J.A.A. Selvan, A.E. Delahoy, S. Guo, Y.-M. Li, *Sol. Energy Mater. Sol. Cells*, 2006, 90, 3371.
- [6] H. Kim, C.M. Gilmore, A. Pique, J.S. Horwitz, D.B. Chrisey, *J. Appl. Phys.* 1999, 11, 6451.
- [7] M. Yan, M. Lane, C.R. Kannewurf, R.P.H. Chang, *Appl. Phys. Lett.* 2001, 78, 2342.
- [8] R.K. Gupta, K. Ghosh, P. Patel, P.K. Kaho, *Appl. Surf. Sci.*, 2009, 255, 6252.
- [9] Vigil, O., Vaillant, L., Cruz, F., Morales-Acevedo, A., Contreras-Puente, G., *Thin Solid Films* 2000,361, 53.
- [10] P.L. Chen, X.Y. Ma, D.S. Li, Y.Y. Zhang, D.R. Yang, *Appl. Phys. Lett.*, 2007, 90, 251115.
- [11] D. Ma, Z. Ye, L. Wang, J. Huang, B. Zhao, *Mater Lett.* 2003, 58, 128.
- [12] L.R. Gutierrez, J.J.C. Romero, J.M.P. Tapia, E.B. Calva, J.C.M. Flores, M.O. Lopez, *Mater. Lett.*, 2006, 60, 3866.
- [13] M. Lorenz, E.M. Kaidashev, H. Von Wenckstern, H. Hochmuth, A. Rahm, H.C. Semmelhack, M. Grundmann, *Solid State Electron.* 2003, 47, 2205.
- [14] Yu Yang, Shu Jin, Julia E. Medvedeva, Arthur J. Freeman, Tobin J. Marks, *J. Am. Chem. Soc.*, 2005, 127, 8796.
- [15] B.J. Zheng, J.S. Lian, L. Zhao, Q. Jiang, *Vacuum*, 2011, 85, 861.
- [16] F.F. Yang, L. Fang, S.F. Zhang, L. Li, G.Z. Fu, *J. Cryst. Growth.*, 2006, 297, 411.

- [17] J.C. Lin, K.C. Peng, C.A. Tseng, S.L. Lee, *Surf. Coat. Technol.*, 2008, 202, 5480.
- [18] R.K. Gupta, K. Ghosha, R. Patel, P.K. Kahol, *J. Alloys Compd.*, 2011, 509, 4146.
- [19] C. Barret, T.B. Massalski, *Structure of Metals*, Petgamon, Oxford, 1980, p1923.
- [20] Y.S. Vidya, K.S. Anantharaju, H. Nagabhushana, S.C. Sharma, *Spectrochim. Acta, Part A*, 2015, 135, 241.
- [21] K.H. Lee, H.W. Jang, K.B. Kim, Y.H. Tak, J.L. Lee, *J. Appl. Phys.*, 2004, 95, 586.
- [22] A.W.C. Lin, N.R. Armstrong, T. Kuwana, *Anal. Chem.*, 1977, 49, 1228.
- [23] F. Javier Yusta, M.L. Hitchman, S.H. Shamlan, *J. Mater. Chem.*, 1997, 7, 1421.
- [24] E. Burstein, *Phys. Rev.*, 1954, 93, 632.
- [25] T. S. Moss, *Optical Properties of Semiconductors* (Butterworths, London, 1961).
- [26] F. Yakuphanoglu, *Appl. Surf. Sci.* 2010, 257, 1413.
- [27] S.H. Werner, H.H. Guttler, *J. Appl. Phys.*, 1991, 69, 1522.
- [28] M. Siad, A. Keffous, S. Mamma, Y. Belkacem, H. Menari, *Appl. Surf. Sci.*, 2004, 236, 366.
- [29] M. Sağlam, A. Ateş, M.A. Yıldırım, B. Güzeldir, A. Astam, *Curr. Appl. Phys.*, 2010, 10, 513.
- [30] A.A.M. Farag, M. Cavas, F. Yakuphanoglu, *Mater. Chem. Phys.*, 2012, 132, 550.
- [31] K.S. Karimov, M.M. Ahmed, S.A. Moiz, M.I. Federov, *Sol. Energy Mater. Sol. Cells*, 2005, 87, 61.
- [32] J. Santos-Cruz, G. Torres-Delgado, R. Castanedo-Pérez, S. Jimenez-Sandoval, J. Márquez-Marín, O. Zelaya-Angel, *Sol. Energy Mater. Sol. Cells*, 2006, 90, 2279.

- [33] S.J.C. Irvine, D.A. Lamb, V. Barrioz, S. Rugen-Hankey, G. Kartopu, *Thin Solid Films*, 2011, 520, 1167.
- [34] Jun Liu, Alexander W. Hains, Jonathan D. Servaites, Mark A. Ratner, Tobin J. Marks, *Chem. Mater.*, 2009, 21, 5258.
- [35] Yanqin Li, Rosanna Mastria, Angela Fiore, Concetta Nobile, Giuseppe Gigli, *Adv. Mater.*, 2009, 21, 4461.
- [36] Bulent M. Basol, Vijay K. Kapur, Michael L. Ferris, *J. Appl. Phys.* 1989, 66, 1816.
- [37] G. Milnes, D.L. Feucht, Academic, New York, 1972.

Table and Figure captions

Table 1 The XPS chemical composition and ratio of oxygen to cadmium for CdO films formed at different Gd and In doping concentrations.

Table 2 The variation of resistivity, carrier concentration and mobility of the undoped and Gd and In doped CdO films.

Table 3 The current density-voltage characteristic results of Al/*n*-Cd_{1-x-y}Gd_xIn_yO/*p*-Si/Ag heterojunction diodes in dark and under 100 mW/cm² illumination power.

Table 4 Comparison of different photovoltaic solar cells obtained by various methods under 100 mW/cm² illumination power. The solar cell parameters are open circuit voltage (V_{oc}), short-circuit current density (J_{sc}), filling factor (FF) and conversion efficiency (η), respectively.

Figure 1 The schematic structure of a nanostructure *n*-CdO/*p*-Si heterojunction diode.

Figure 2 XRD patterns of the CdO films deposited at different Gd and In doping concentrations.

Figure 3 Typical XPS spectra of the CdO films deposited at different Gd and In doping concentrations: (a) survey spectra, and (b, c, d) narrow scan spectra showing (b) Cd 3d, (c) Gd 4d, (d) In 3d.

Figure 4 XPS O 1s signals from the CdO films deposited at different Gd and In doping concentrations: (a) undoped, (b) 1 at.% Gd and 2 at.% In, (c) 2 at.% Gd and 4 at.% In, and (d) 3 at.% Gd and 6 at.% In.

Figure 5 FESEM images of the CdO films deposited at different Gd and In doping concentrations: (a) undoped, (b) 1 at.% Gd and 2 at.% In, (c) 2 at.% Gd and 4 at.% In, and (d) 3 at.% Gd and 6 at.% In.

Figure 6 Optical transmission spectra of the CdO films deposited at different Gd and In doping concentrations on quartz glass substrate. The inset image shows the relation between $(ah\nu)^2$ and $h\nu$ of the sample films.

Figure 7 Current density-voltage (J - V) characteristics of the $\text{Al}/n\text{-Cd}_{1-x-y}\text{Gd}_x\text{In}_y\text{O}/p\text{-Si}/\text{Ag}$ heterojunction diodes in dark. The inset image shows the rectification ratio dependence of the applied bias.

Figure 8 Current density-voltage (J - V) characteristic in a double logarithmic plot for the $\text{Al}/n\text{-Cd}_{1-x-y}\text{Gd}_x\text{In}_y\text{O}/p\text{-Si}/\text{Ag}$ heterojunction diodes in SCLC region. The inset image shows dopant content dependence of the slope m .

Figure 9 Current density-voltage (J - V) characteristics of $\text{Al}/n\text{-Cd}_{1-x-y}\text{Gd}_x\text{In}_y\text{O}/p\text{-Si}/\text{Ag}$ heterojunction diodes under $100 \text{ KW}/\text{cm}^2$ illumination power.

Figure 10 Schematic energy band diagrams of the $\text{Al}/n\text{-Cd}_{1-x-y}\text{Gd}_x\text{In}_y\text{O}/p\text{-Si}/\text{Ag}$ heterojunction diode under the dark and illumination condition, respectively.

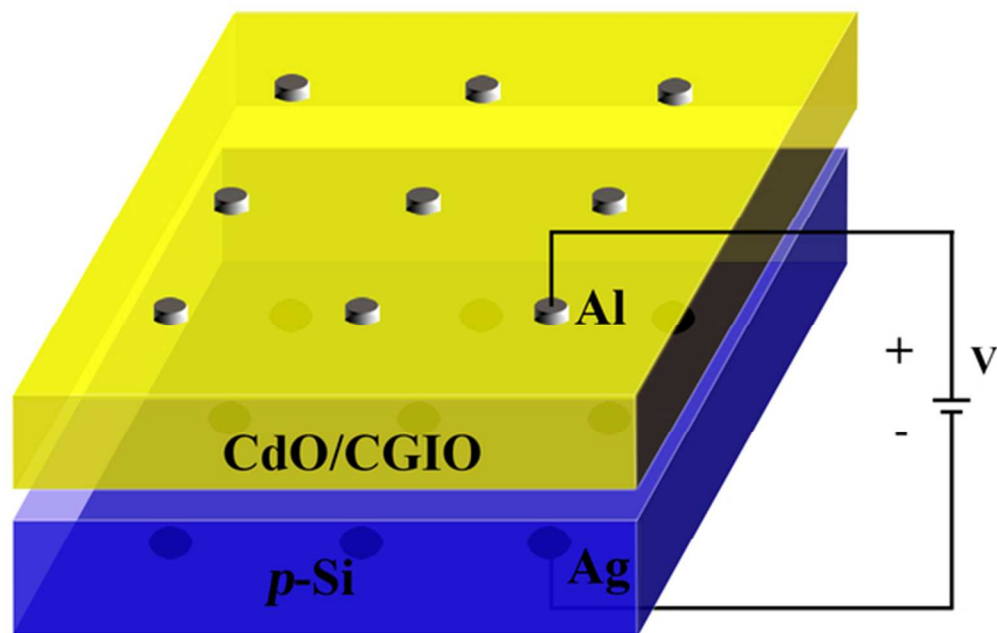
Figure 11 The band structure of the $\text{Al}/n\text{-Cd}_{1-x-y}\text{Gd}_x\text{In}_y\text{O}/p\text{-Si}/\text{Ag}$ heterojunction diode under forward bias.

Table 2

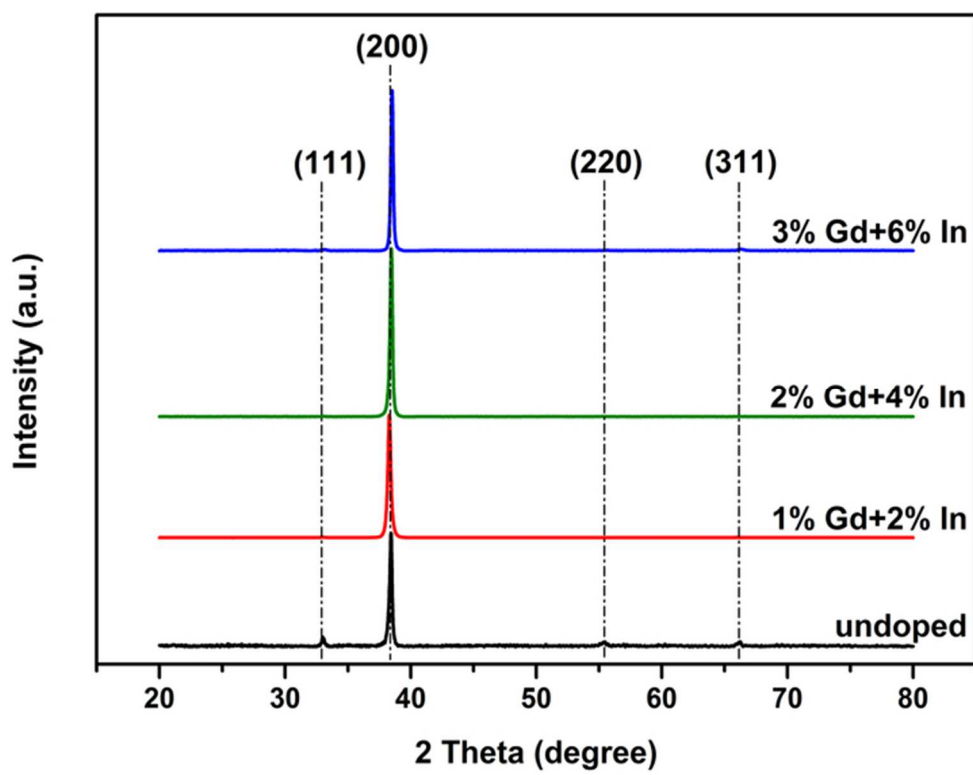
Sample No.	Electrical properties		
	ρ ($\times 10^{-4}$ Ωcm)	n ($\times 10^{20}$ cm^{-3})	μ (cm^2/Vs)
CdO	24.8	1.08	77.5
CGIO-1	6.85	3.84	84.6
CGIO-2	1.92	9.7	96.5
CGIO-3	0.76	14.7	115.9

Table 4

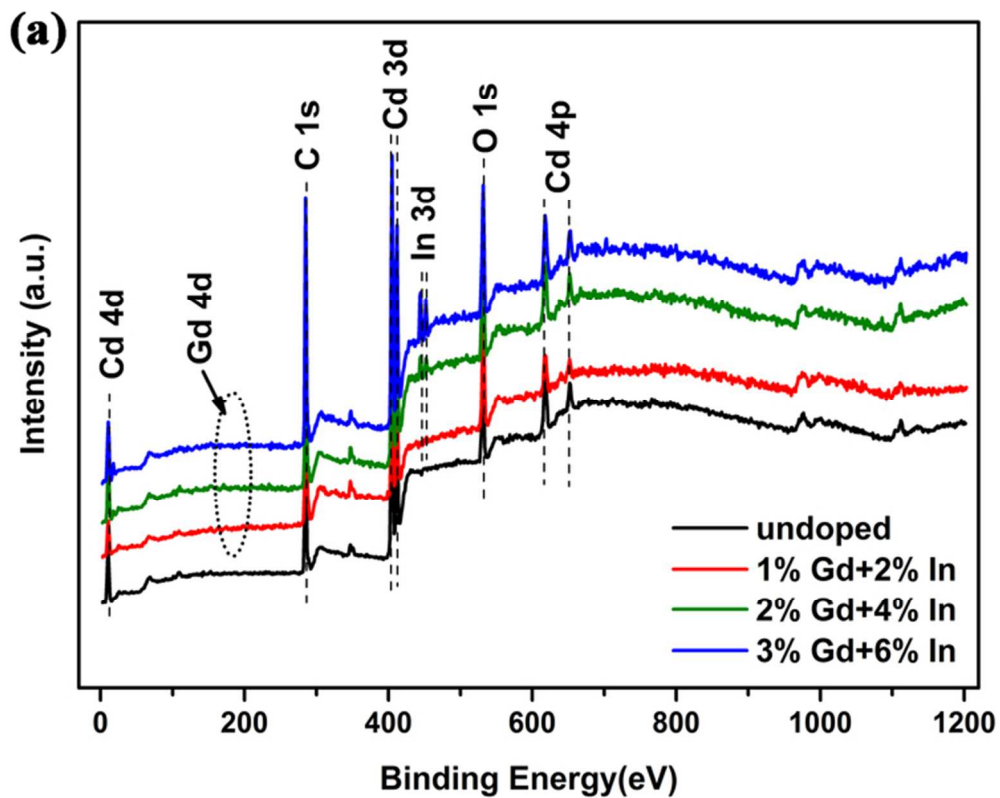
Sample	V_{oc} (V)	J_{sc} (mA/cm ²)	FF (%)	η (%)	Reference
CdFO/CdSbTe	0.52	28.6	33	5.48	[34]
CdZnS/CdTe	0.71	22.5	68	10.9	[35]
CdInO/ITO	0.82	3.49	52	1.49	[36]
CdSe@CdTe-C60/ITO	0.43	3.15	46	0.62	[37]
CdS/CdZnTe	0.55	15	45	3.8	[38]
CGIO-3	1.04	11.4	63	7.5	present



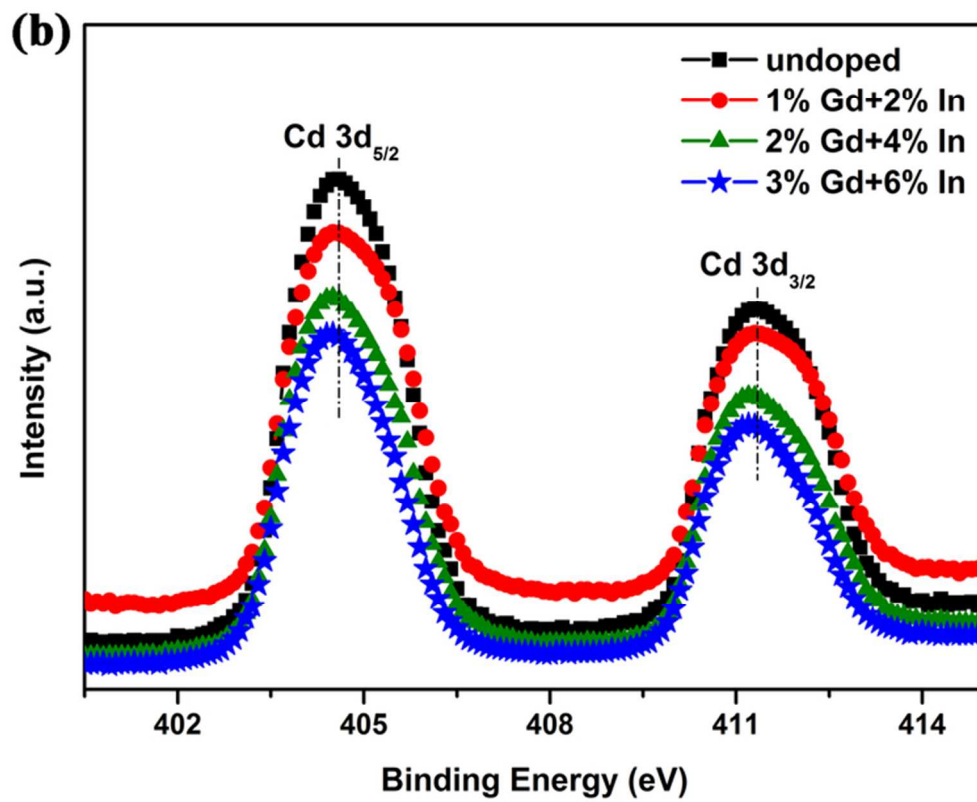
51x33mm (300 x 300 DPI)



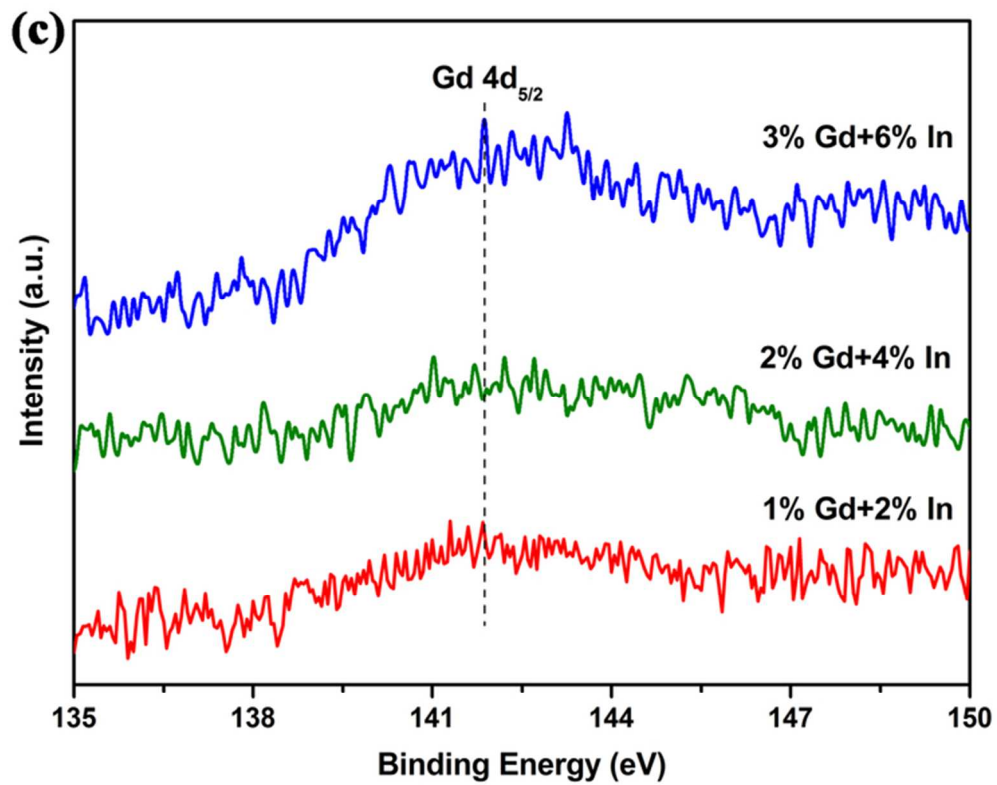
62x49mm (300 x 300 DPI)



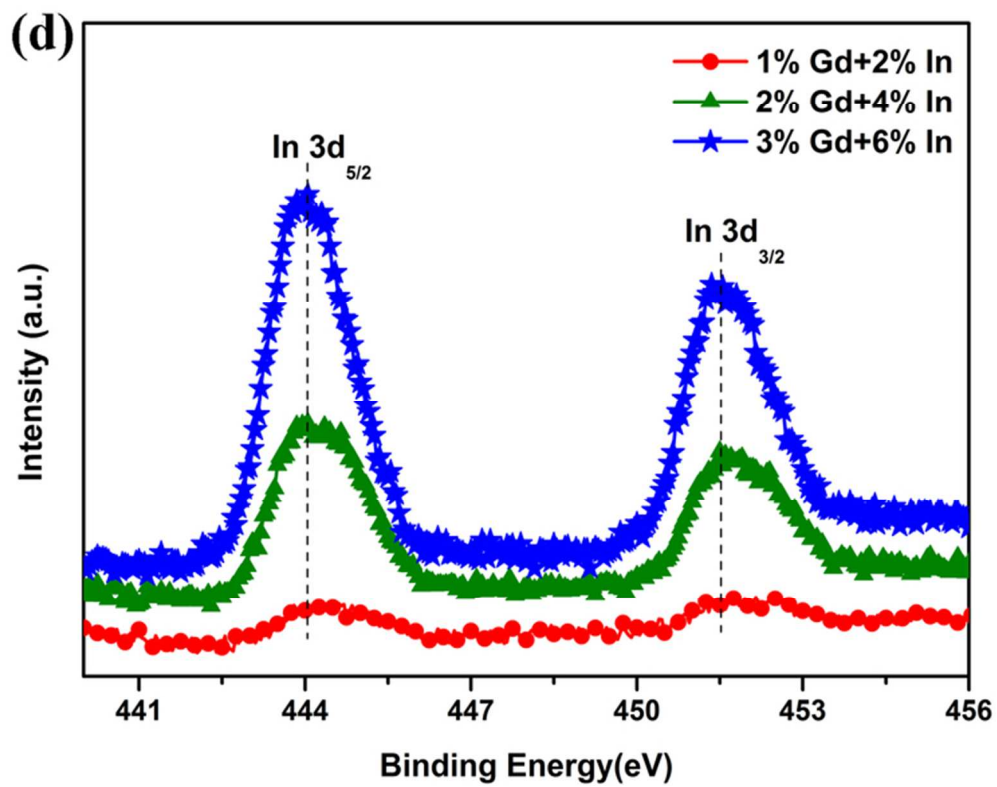
63x51mm (300 x 300 DPI)



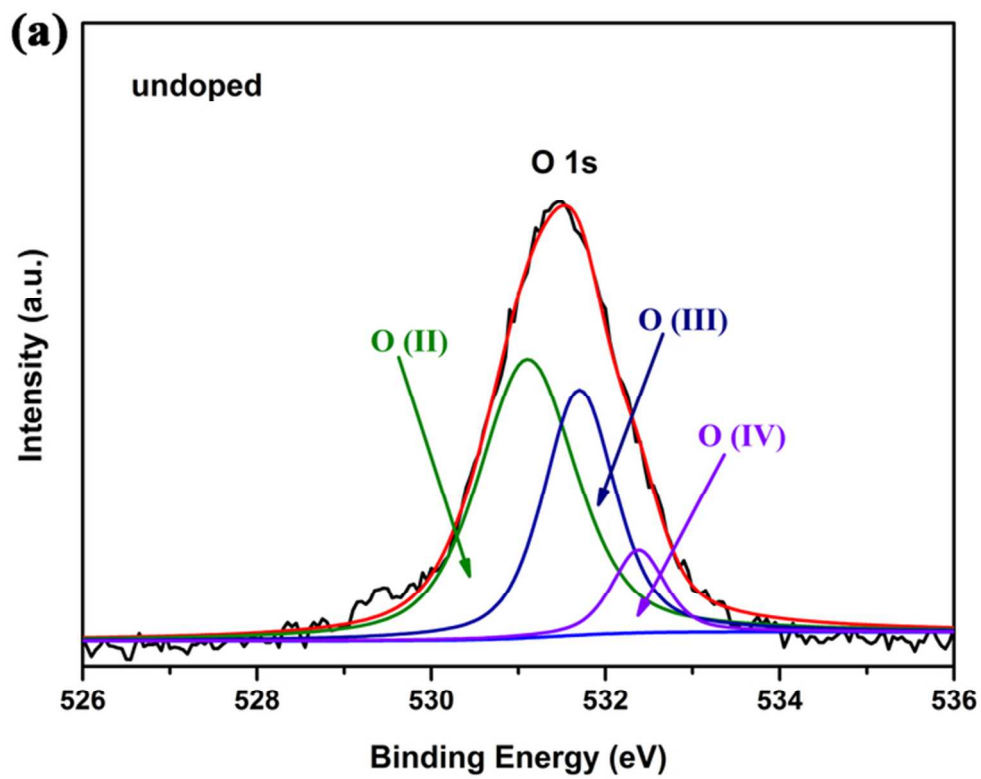
64x52mm (300 x 300 DPI)



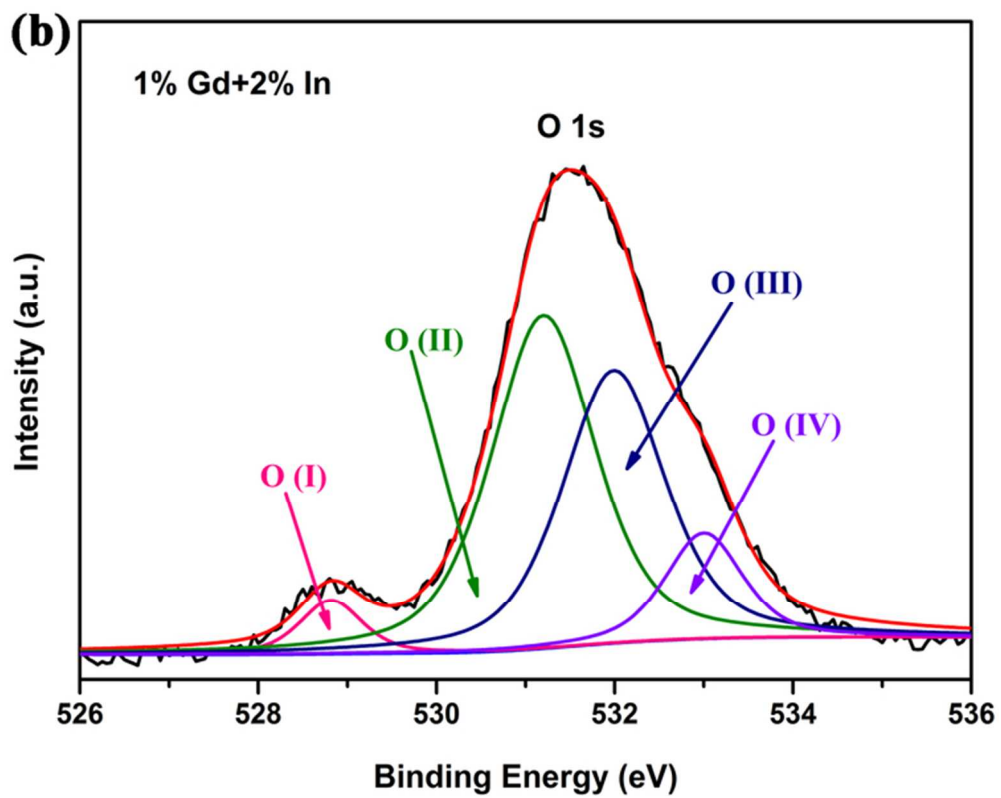
63x49mm (300 x 300 DPI)



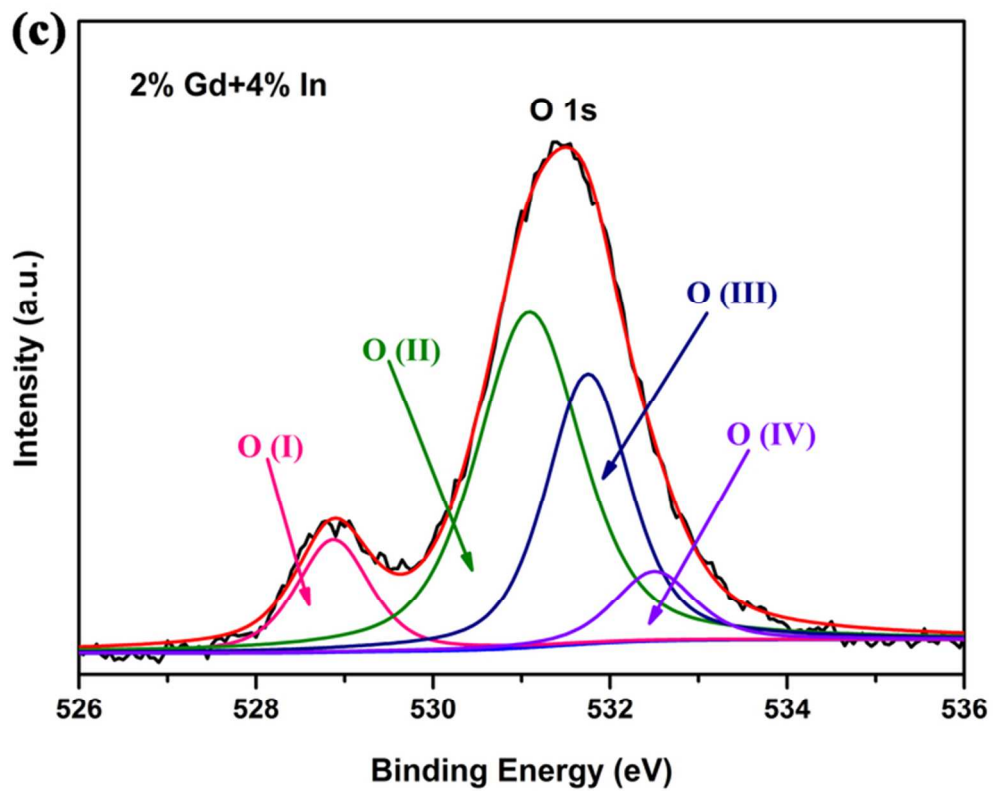
63x50mm (300 x 300 DPI)



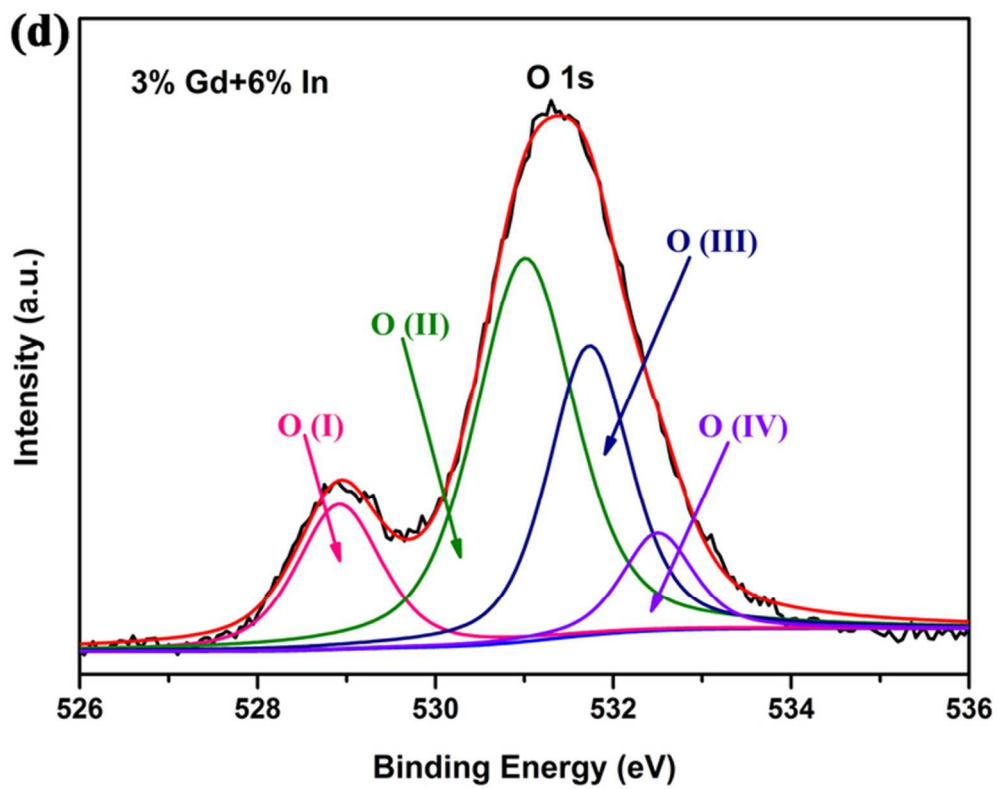
62x49mm (300 x 300 DPI)



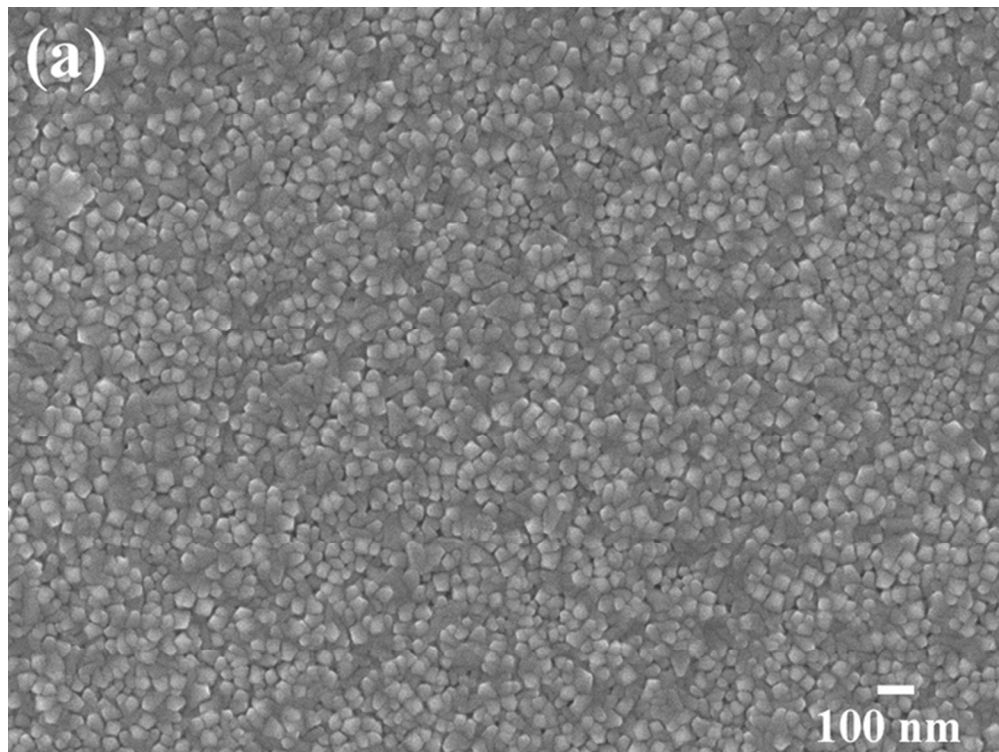
64x51mm (300 x 300 DPI)



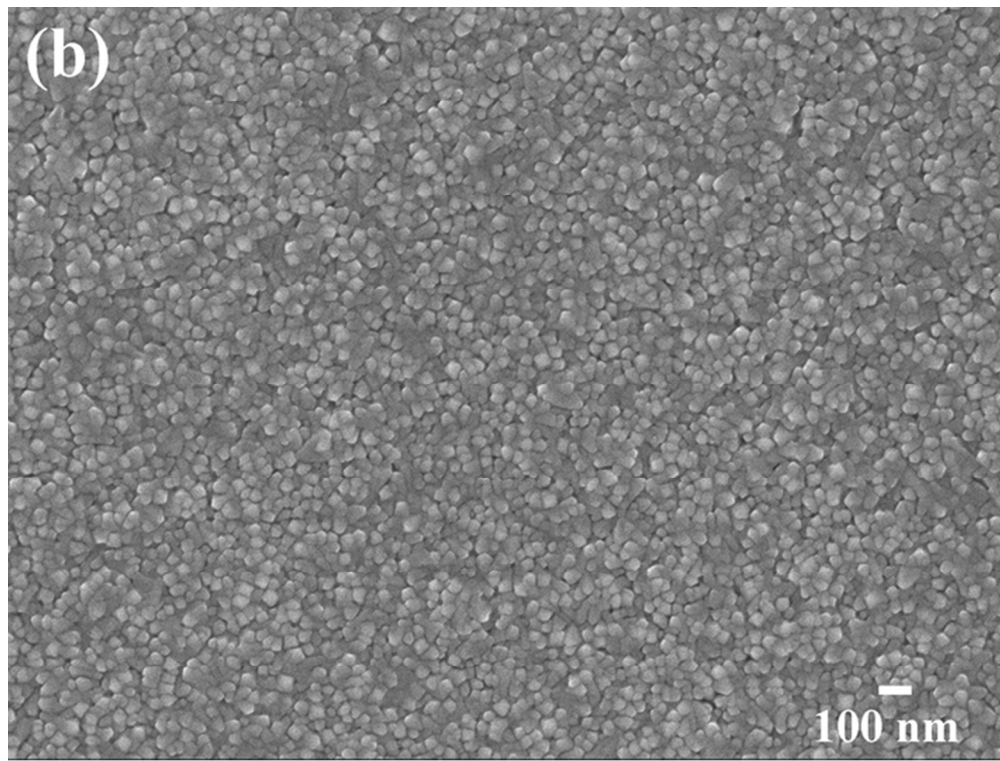
63x50mm (300 x 300 DPI)



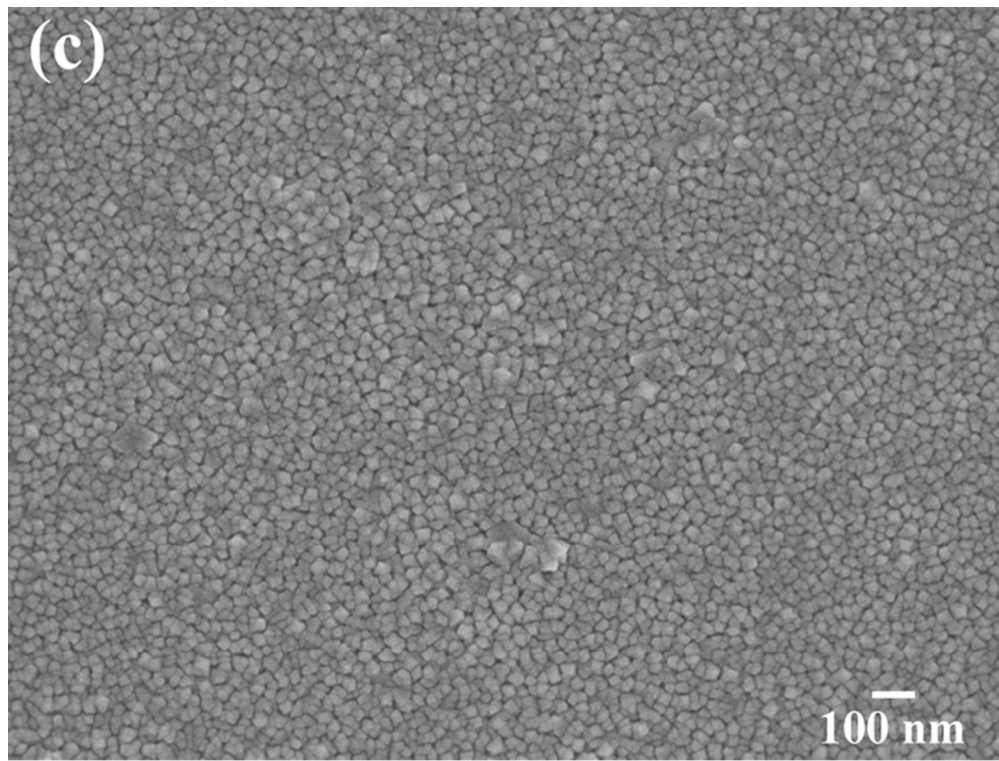
62x49mm (300 x 300 DPI)



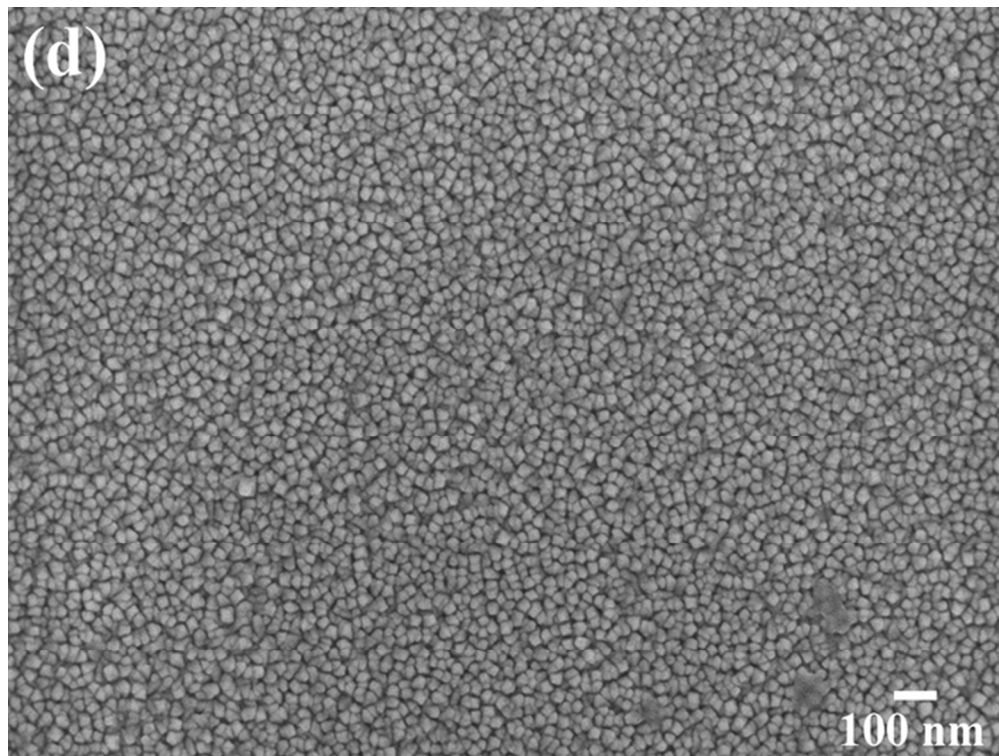
59x44mm (300 x 300 DPI)



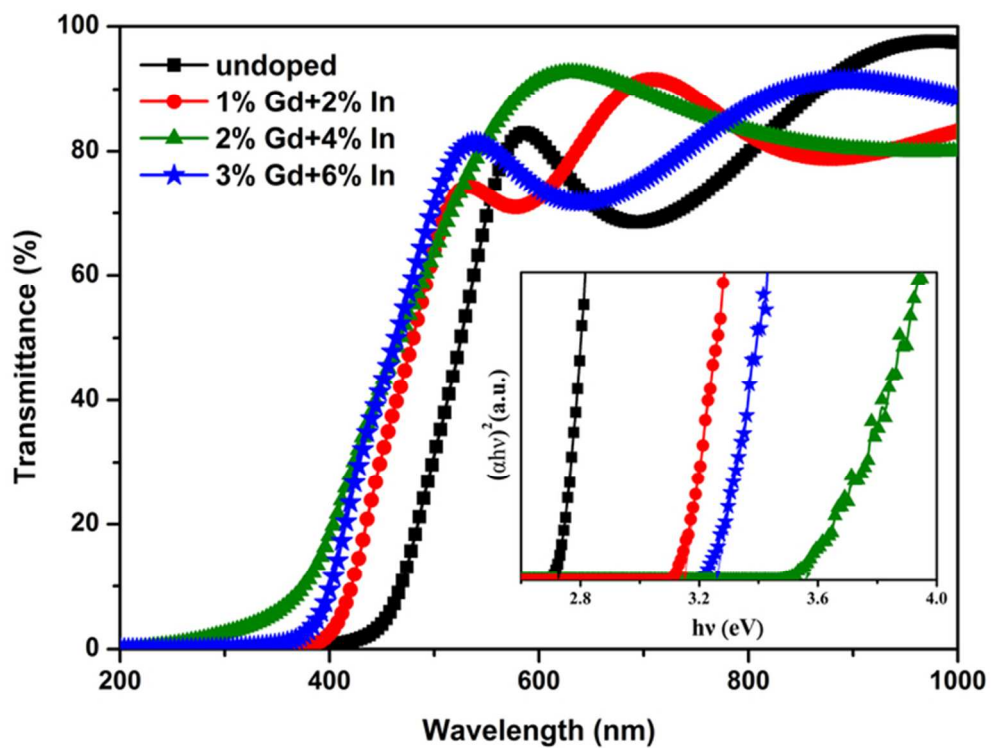
60x45mm (300 x 300 DPI)



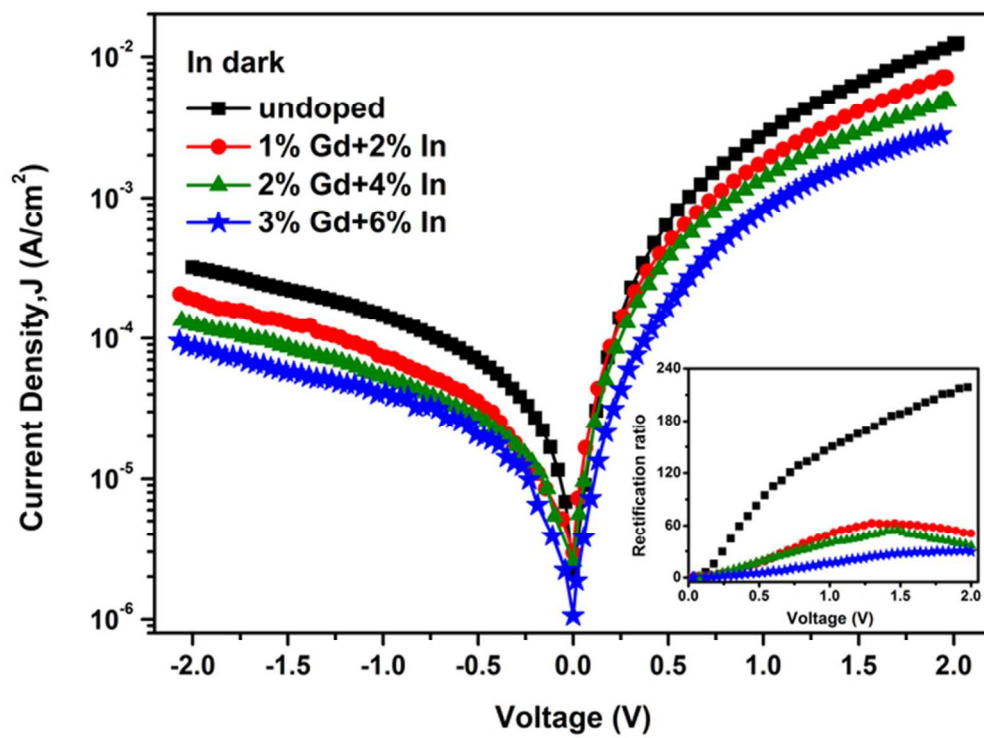
60x45mm (300 x 300 DPI)



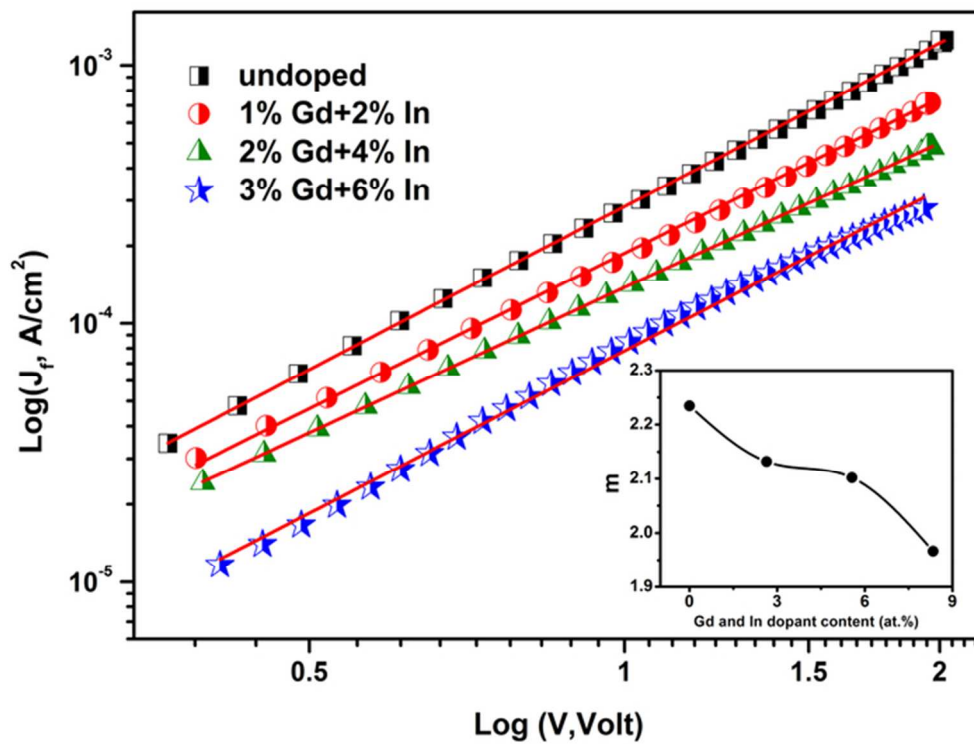
59x44mm (300 x 300 DPI)



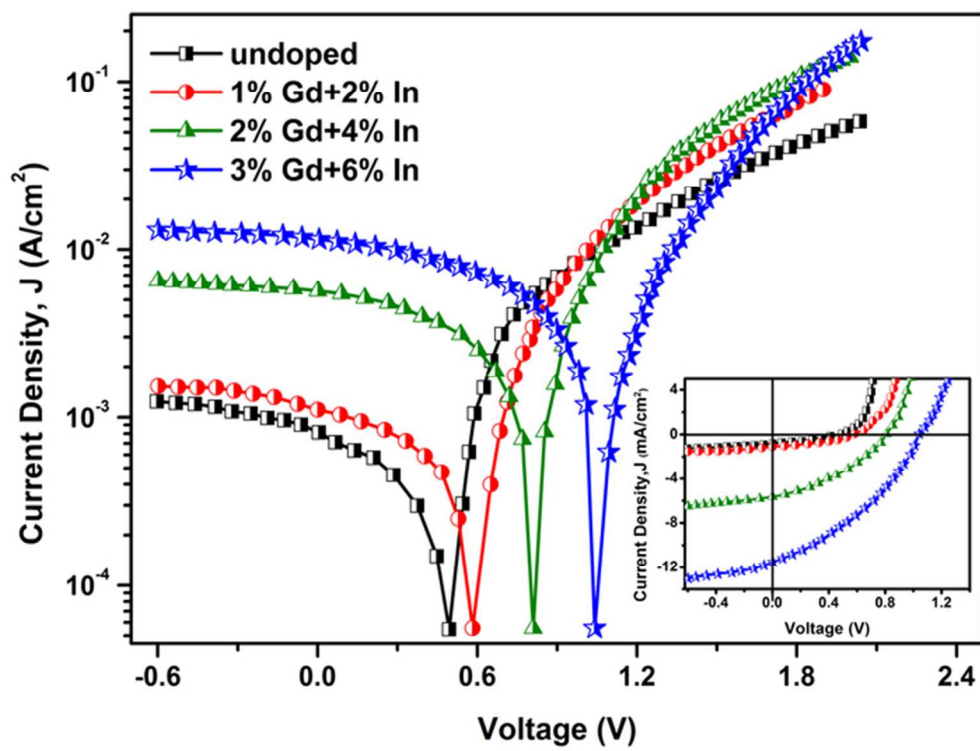
60x46mm (300 x 300 DPI)



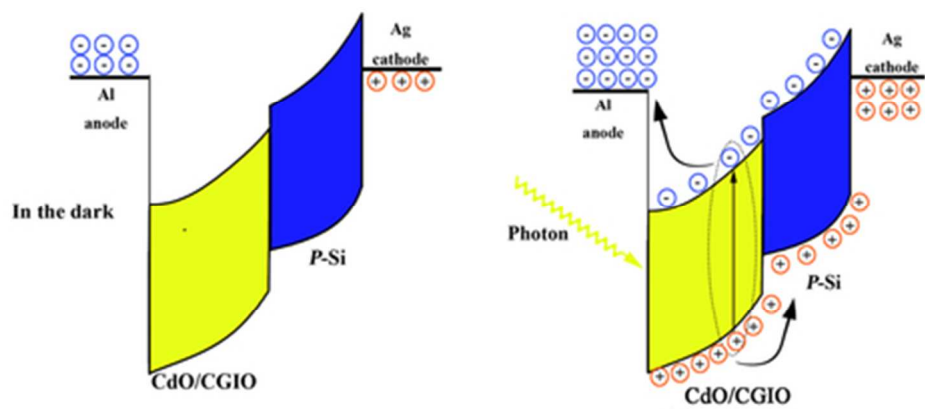
59x44mm (300 x 300 DPI)



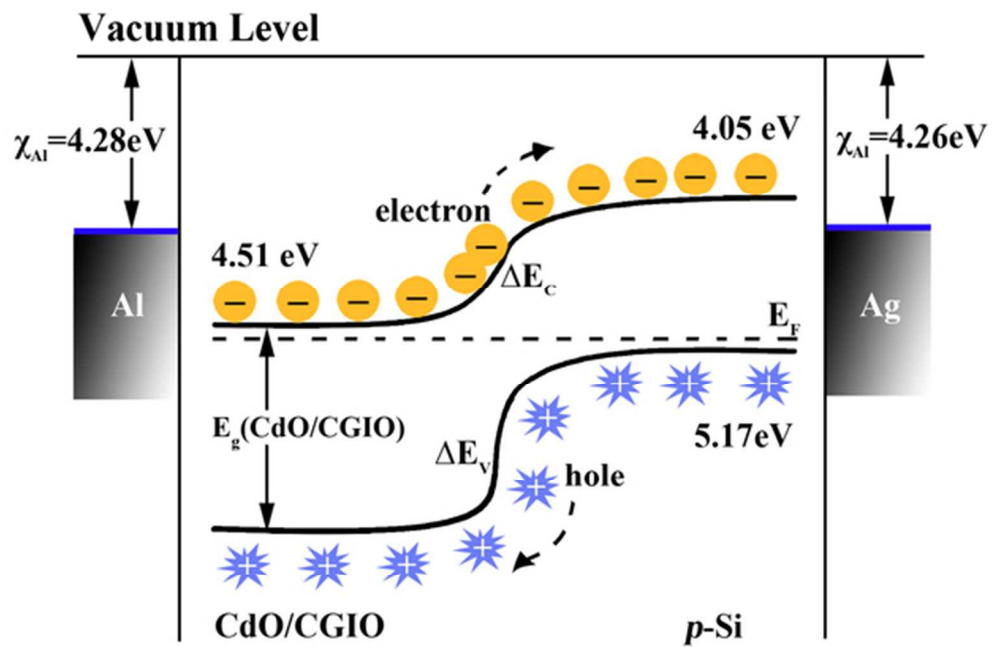
60x45mm (300 x 300 DPI)



60x45mm (300 x 300 DPI)



39x17mm (300 x 300 DPI)



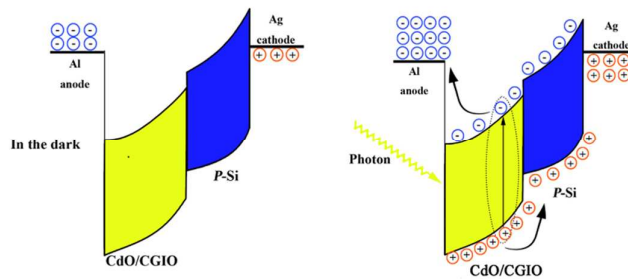
53x35mm (300 x 300 DPI)

Table 1

Sample No.	Nominal % of dopant in target material		Dopant % from XPS in thin films		[O]/[Cd]
	Gd	In	Gd	In	
CdO	0	0	0	0	0.81
CGIO-1	1	2	0.75	1.89	0.85
CGIO-2	2	4	1.79	3.77	0.89
CGIO-3	3	6	2.65	5.69	0.94

Table 3

Sample No.	Dark			Illumination							
	n	Φ_b (eV)	R_s ($\Omega \cdot \text{cm}^2$)	R_{sh} ($\Omega \cdot \text{cm}^2$)	R_s ($\Omega \cdot \text{cm}^2$)	R_{sh} ($\Omega \cdot \text{cm}^2$)	V_{oc} (V)	J_{sc} (mA/cm^2)	FF (%)	η (%)	S (mA/W)
CdO	2.27	0.55	161.2	6215.8	34.5	483.9	0.49	0.8	51	0.2	45.6
CGIO-1	2.11	0.57	272.2	9978.6	21.1	392.2	0.58	1.1	52	0.3	828.3
CGIO-2	1.93	0.58	410.4	15318.6	14.2	92.3	0.80	5.6	59	2.6	1357.9
CGIO-3	1.69	0.61	689.3	21657.2	11.8	46.2	1.04	11.4	63	7.5	1708



Graphical Abstract

The Al/n-CdO:Gd:In/p-Si/Ag heterojunction diode showed excellent photoelectrical property and was suitable for solar cell applications.